THE JOURNAL OF PHYSICAL CHEMISTRY B
A JOURNAL OF THE AMERICAN CHEMICAL SOCIETY

pubs.acs.org/JPCB

Article

Topological Constraints with Optimal Length Promote the Formation of Chromosomal Territories at Weakened Degree of Phase Separation

Published as part of The Journal of Physical Chemistry virtual special issue "125 Years of The Journal of Physical Chemistry".

Jiachen Wei,* Hao Tian, Rui Zhou, Yingfeng Shao, Fan Song, and Yi Qin Gao*

Cite This: https://doi.org/10.1021/acs.jpcb.1c03523

Read Online

ACCESS | Metrics & More | Article Recommendations | Supporting Information

ABSTRACT: It is generally agreed that the nuclei of eukaryotic cells at interphase are partitioned into disjointed territories, with distinct regions occupied by certain chromosomes. However, the underlying mechanism for such territorialization is still under debate. Here we model chromosomes as coarse-grained block copolymers and to investigate the effect of loop domains (LDs) on the formation of compartments and territories based on dissipative particle dynamics. A critical length of LDs, which depends sensitively on the length of polymeric blocks, is obtained to minimize the degree of phase separation. This also applies to the two-polymer system: The critical length not only maximizes the degree of territorialization but also minimizes the degree of phase separation. Interestingly, by comparing with experimental data, we find the critical length for LDs and the corresponding length of blocks to be respectively very close to the mean length of topologically associating domains (TADs) and chromosomal segments with different densities of CpG islands for human chromosomes. The results indicate that topological constraints with optimal length can contribute to the formation of territories by weakening the degree of phase separation, which likely promotes the chromosomal flexibility in response to genetic regulations.

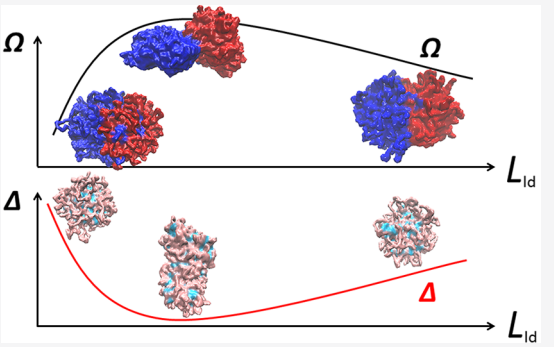

INTRODUCTION

Rather than randomly distributed coils, chromosomes are of a hierarchical architecture[1−11] for high compaction, fast unfolding, and easy unentanglement. The hierarchy of structure includes (but is not limited to) the formation of topologically associating domains (TADs), intrachromosomal compartments, and territories for individual chromosomes. TADs correspond to local regions of typical lengths ranging from 40 kb to 1Mb in which self-contacts are enhanced and spatially confined.[8,12] At the megabase scale, chromatin that differs in gene distributions, density, or epigenetic marks segregates into two compartments.[5,13−17] Aside from other potential drivers (e.g., bridging-induced attraction for proteins[18] and preferential binding of HP1 to regions high in histone methylation),[19] liquid-phase separation mediated by weak hydrophobic interactions are argued to play a critical role in the formation of compartments.[20,21] This could originate from heterogeneity in the densities of CpG islands[16,17] (CGIs) for genomic segments. At the nuclei scale, individual chromosomes occupy their own space,[1−5,22−26] resulting in significantly more intrachromosomal than interchromosomal contacts.

The underlying mechanism for the formation of territories remains unclear so far. One proposed mechanism assumes an activity-based dynamics,[27] for which gene-rich euchromatin and gene-poor heterochromatin are respectively represented by active and inert chains. However, it has been demonstrated[28] that a quasi-equilibrium model without a difference in activity is adequate to mimic the dynamics of the chromosomes in vivo.[29−31] The structure of chromatin within territories is nonrandom due to the presence of TADs and compartments, which probably contributes to the formation of territories.[22] The multiscale chromatin structures have a territorial organization by nature: Segments close to each other along the chromosome are close to each other in space as well.[3,22] Nevertheless, how different structures interfere has rarely been discussed so far. Recent studies have shown that TADs play a

Received: April 19, 2021
Revised: July 19, 2021

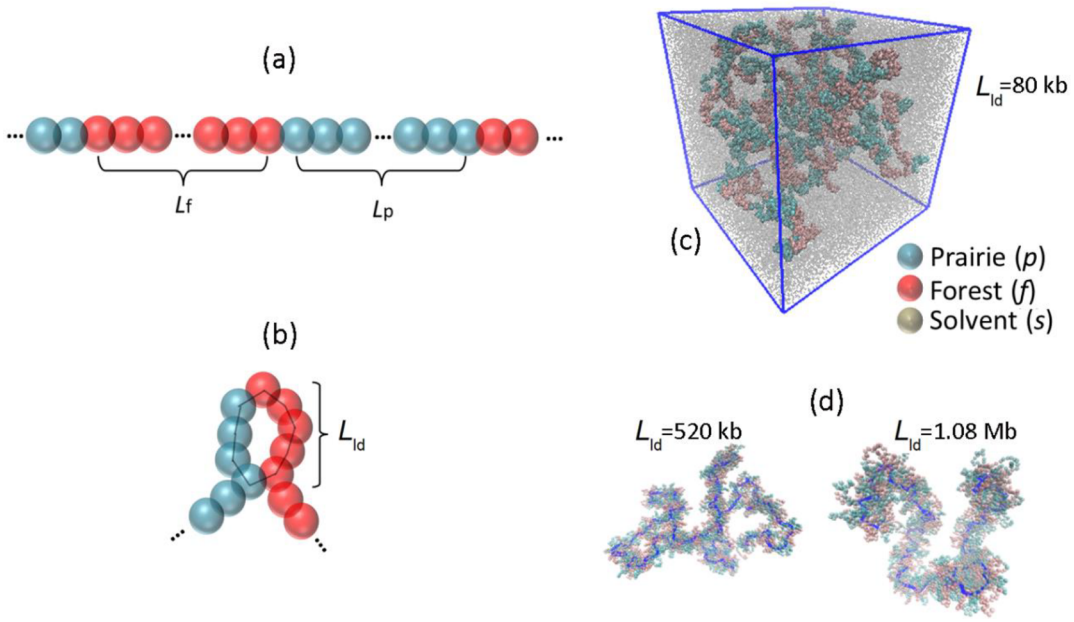

Figure 1. (a) Sketch of the polymer model for chromosome. The bead is in type of either forest (f) or prairie (p), with different hydrophobicity. L_f and L_p respectively denote the length for consecutive forest and prairie beads. (b) Sketch of one LD on a polymer, with L_{ld} denoting the length of the LD. (c) Simulation snapshot of a −50−50− polymer with L_{ld} = 80 kb in solvent before collapsing. (d) Simulation snapshots of −50−50− polymers with L_{ld} = 520 kb and L_{ld} = 1.08 Mb. The backbones are indicated by blue solid lines.

competing role with compartmental phase separation, instead of building blocks for compartments.[14,32−35] Quantitative analysis is still in need to unveil the basic mechanisms of this competing relation. The potential influence of TADs on the formation of territories is to be investigated, but the formation of territories of ring polymers[6,36] has implied the assisting effects of topological constraints. The effect of loop size on territory formation has also been proposed[23,24] but not much investigated in depth.

Various coarse-grained models have been proposed to capture and interpret complex features of chromosomes emerging from experiments.[37−42] In this work, we start from a bead-and-spring coarse-grained model, which is commonly used to investigate structural properties of compartments and domains.[14,43,44] The hydrophobic interactions are introduced based on the dissipative particle dynamics (DPD), which were implemented in earlier studies to analyze the folding of fractal globules and chromosomes.[31,45−48] Without a loss of generality, the model is applied to study the interplay of multiscale structures for human chromosomes, based on experimental results for TAD boundaries and genomic sequence. The results indicate the existence of an optimal length of TADs that maximizes the degree of territorialization and meanwhile minimizes the degree of phase separation. In the remainder of this paper, we first introduce the simulation methods before presenting the results. Taking a polymer of periodic blocks as an example, we are particularly interested in the dependence of phase separation and territory formation on topological constraints. Next, we study the effect of topological constraints on compartmentalization and territorialization for human chromosomes, followed by conclusions.

SIMULATION METHOD

Model. We perform DPD simulations of coarse-grained polymers submerged in solvent. The polymer is modeled as a chain of DPD beads of total length L. As shown in Figure 1, the polymeric bead is either of the type forest (f) or prairie (p), which corresponds to chromosomal segments with either rich or poor densities of CGIs, respectively. The solvent (s) is explicitly modeled as DPD beads of the same size as f and p. The polymer is of periodic blocks with repeat units of n_f forest beads followed by n_p prairie beads, denoted as "$-n_f-n_p-$". The curvilinear lengths of the forest and prairie segments are denoted as L_f and L_p respectively. As illustrated in Figure 1b, topological constraints are introduced by cross-linking non-adjacent beads at fixed distance L_{ld}, forming consecutive loop domains (LDs). This is to phenomenologically model the TADs of chromosomes at comparable length scales. To test the effect of LD lengths, the $-n_f-n_p-$ polymer is of a fixed L_{ld} ranging from 0.0 to 1.96 Mb (L_{ld} = 0 denoting system without LDs). Since the LD boundaries are consecutive (without open segments between loops), the total number of LDs on a polymer $N_{ld} = L/L_{ld}$. The model is then applied to simulate human chromosomes (with each bead representing about 40 kb segments), for which disordered distributions of $L_{f,p}$ and L_{ld} are respectively derived from genomic sequence and TAD boundaries.[16,17,49−51] See the Supporting Information for more details.

All beads (s, f, and p) interact with each other via DPD interactions, including a conservative force $\mathbf{F}_{ij}^{C}$, a dissipative force $\mathbf{F}_{ij}^{D}$, and a random force $\mathbf{F}_{ij}^{R}$ given by

$$\begin{aligned}
\mathbf{F}_{ij}^{C} &= A_{ij}(1 - r_{ij}/r_c)\mathbf{e}_{ij} \quad \text{for } r_{ij} < r_c \\
\mathbf{F}_{ij}^{D} &= -\gamma_{ij}(1 - r_{ij}/r_c)^2(\mathbf{e}_{ij}\cdot\mathbf{v}_{ij})\mathbf{e}_{ij} \quad \text{for } r_{ij} < r_c \\
\mathbf{F}_{ij}^{R} &= -\sqrt{2k_BT\gamma_{ij}}(1 - r_{ij}/r_c)\,\theta_{ij}(\delta t)^{-1/2}\,\mathbf{e}_{ij} \quad \text{for } r_{ij} < r_c
\end{aligned} \tag{1}$$

where r_{ij} is the center-to-center distance between beads i and j, $\mathbf{e}_{ij} = \mathbf{r}_{ij}/r_{ij}$ the unit vector, A_{ij} is the maximum repulsion, γ_{ij} is the dissipative constant, $\mathbf{v}_{ij}$ is the vector difference in velocities

https://doi.org/10.1021/acs.jpcb.1c03523
J. Phys. Chem. B XXXX, XXX, XXX−XXX

between the two beads, θ_{ij} is a Gaussian white noise variable with $\theta_{ij} = \theta_{ji}$, and δt is the simulation time step. All these three forces vanish when $r_{ij} \geq r_c$. As a common choice for DPD parameters,[47,52,53] we set $A_{ij} = 150$ and $\gamma_{ij} = 4.5$ between all DPD beads (except for a slightly larger A_{sp} for phase separation). By increasing A_{sp} from 150 to 170, the effective Flory–Huggins parameter[52] $\chi_{sp} = 0.306(A_{sp} - A_{pp})$ varies from 0.0 to 6.1. See Table 1 for the full list of interaction parameters used in this paper (unless otherwise specified).

Table 1. Parameters for Interactions between Different Types of Beads

bonded interactions	K	r_0	
f/p–f/p	150	0.5	
DPD interactions	A_{ij}	γ_{ij}	r_c
f/p–f/p	150	4.5	1.0
s–f	150	4.5	1.0
s–p	varied	4.5	1.0

Bonded forces are added to the model describing chain connectivity, which can be written as

$$\mathbf{F}_{ij}^{B} = -K(r_{ij} - r_0)\mathbf{e}_{ij} \tag{2}$$

with $K = 150$ and $r_0 = 0.5$ respectively representing the spring constant and equilibrium bond length. Equation 2 is also used for modeling bonded interactions between LD boundaries (i.e., nonadjacent beads that are cross-linked). We assume the formation of a fractal globule with topological constraints (i.e., the chain cannot cross itself).[3] This can be achieved[31,54] by allowing $\sqrt{2}d_{min} > l_{max}$, with d_{min} and l_{max} respectively denoting the minimum distance between two beads and maximum bond length for consecutive beads. With our choice of interaction parameters, at least 94% of the contacting pairs ($r_{ij} < r_c$) meet the requirement.

The cutoff radius of the DPD bead r_c, the system time τ, system temperature T, and the corresponding energy k_BT (where k_B is the Boltzmann constant) are chosen as the reduced units, which (approximately) correspond to $\hat{r}_c = 200$ nm, $\hat{\tau} = 5.1$ μs, $\hat{T} = 298$ K, and $k_B\hat{T} = 4.11 \times 10^{-21}$ J in real units to match experimental results for human chromosomes (see the Supporting Information). Unless specified, reduced units will be used in the remainder of this paper.

Simulation Details. We first simulate a submerged $-n_f-n_p-$ polymer of total length $L = 228$ Mb in a $29.4 \times 29.4 \times 29.4$ cubic box with periodic boundary conditions implemented in all three dimensions; see Figure 1c. To make simulation box impermeable for polymer, an additional wall interaction $\mathbf{F}_i^W$ is implemented between the boundary box and polymeric bead i:

$$\mathbf{F}_i^W = -K_w(r_{iw} - r_c^w)\mathbf{e}_w \quad \text{for } r_{iw} < r_c^w \tag{3}$$

with $K_w = 150$ and $r_c^w = 0.5$, $\mathbf{e}_w$ being the unit vector in normal direction of the wall. The simulation box is sufficiently large so that the degree of phase separation is barely affected by $\mathbf{F}_i^W$. The volume fraction of polymers (5–20%) agrees with that for chromosomes in cell nucleus[6] (2–30%).

All simulations are carried out by the parallel software package LAMMPS.[55] The velocity–Verlet algorithm with a time step of $\delta t = 0.02$ is used to integrate the equations of motion. The initial configuration of the polymer is generated by self-avoiding random walk (SAW) with a unit walk length $l = 0.7$ at each step in the cubic box. A total number of N_s solvent beads (s) is maintained at fixed density $\rho_s = 3.0$ and temperature $T = 1.0$ in the NVT ensemble. We first simulate a homopolymer with $A_{sf} = A_{sp} = 150$ and perform at least 5×10^6 simulation steps for equilibration. Subsequently, a slightly larger A_{sp} is implemented for phase separation. The equilibrium state is achieved after the potential energy of the collapsed polymer becomes stable during a sufficiently long run. The trajectories for the collapsed or semicollapsed polymer are obtained and analyzed in the next 4×10^7 simulation steps. The results are averaged over at least 20 independent runs each initiated from independent conformations.

The degree of phase separation of f and p beads can be quantified[14] by the order parameter Δ, which is defined as

$$\Delta = \frac{\sum_{S=1}^{L/2} \langle (\xi_S^{same} - \xi_S^{diff})/(\xi_S^{same} + \xi_S^{diff}) \rangle}{L/2} \tag{4}$$

where ξ_S^{same} and ξ_S^{diff}, respectively, represent the ratio of contacting bead pairs ($r_{ij} < r_c$) among all possible pairs in same and different types at curvilinear distance $S = i - j$ along the chain. By definition, Δ measures the relative difference in same-type and different-type contact probabilities. By weighing all distances from the main diagonal equally, Δ is insensitive to the total length of the polymer[14] (i.e., no scaling effect). Note that the degree of phase separation can also be quantitatively measured via other methods, such as the modularity of the community based on graph theory.[56,57] See the Supporting Information for more discussions.

The same simulation box is used for analyzing the formation of territories between two $-50-50-$ polymers of length $L_\alpha = 228$ Mb and $L_\beta = 240$ Mb. Initially, the box is divided into two subcompartments to separately generate the initial configurations of the two polymers without unreasonable entanglement. Simulations of 5×10^6 steps are performed at fixed $A_{sp} = 150$ with each polymer occupying one subcompartment by applying wall interactions F_i^W between compartment and the polymers. Next, the subcompartments are removed, and A_{sp} is increased. After equilibrating for at least 2×10^7 simulation steps, the contact map is analyzed in the following 4×10^7 simulation steps. To quantitatively characterize the degree of territorialization between two polymers, we define the order parameter Ω as

$$\Omega = (P^{same} - P^{diff})/(P^{same} + P^{diff}) \tag{5}$$

with

$$P^{same} = \frac{\sum_{i=1}^{L_\alpha - L_{ld}} \sum_{j=i+L_{ld}}^{L_\alpha} P_{ij}}{0.5(L_\alpha - L_{ld})(L_\alpha - L_{ld} + 1)} + \frac{\sum_{i=1+L_\alpha}^{L_\alpha + L_\beta - L_{ld}} \sum_{j=i+L_{ld}}^{L_\alpha + L_\beta} P_{ij}}{0.5(L_\beta - L_{tad})(L_\beta - L_{ld} + 1)}$$

$$P^{diff} = \frac{\sum_{i=1+L_\alpha}^{L_\alpha + L_\beta} \sum_{j=1}^{L_\alpha} P_{ij}}{L_\alpha L_\beta} \tag{6}$$

Here P^{same} and P^{diff} respectively denote the probabilities of intra- and interpolymeric contacts, which can be determined from the contact map by averaging over contact probability P_{ij} for each bead pair i and j. A larger cutoff radius $r_c^{map} = 6.0$ is implemented for measuring P_{ij} with enhanced contrast. Pairs

https://doi.org/10.1021/acs.jpcb.1c03523
J. Phys. Chem. B XXXX, XXX, XXX–XXX

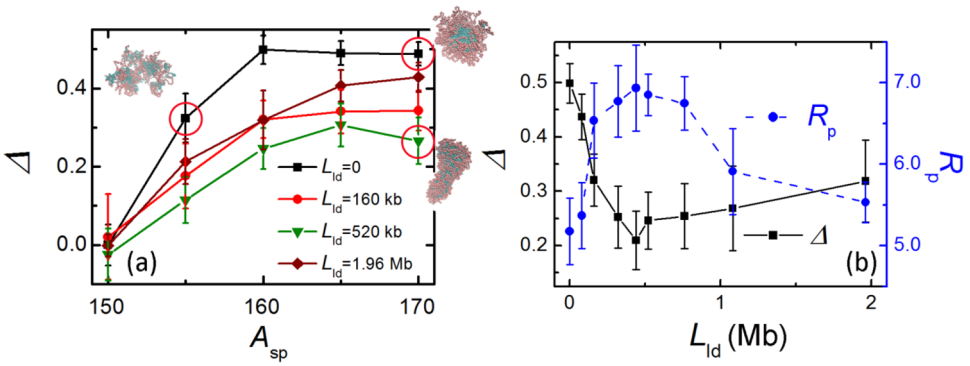

Figure 2. (a) Degree of phase separation of f and p compartments, Δ, as a function of solvent−prairie repulsion, A_{sp}, for −50−50− polymer. Typical simulation snapshots are indicated by red circles. (b) Dependence of Δ and gyration radius of prairie beads R_p on L_{ld} at A_{sp} = 160.

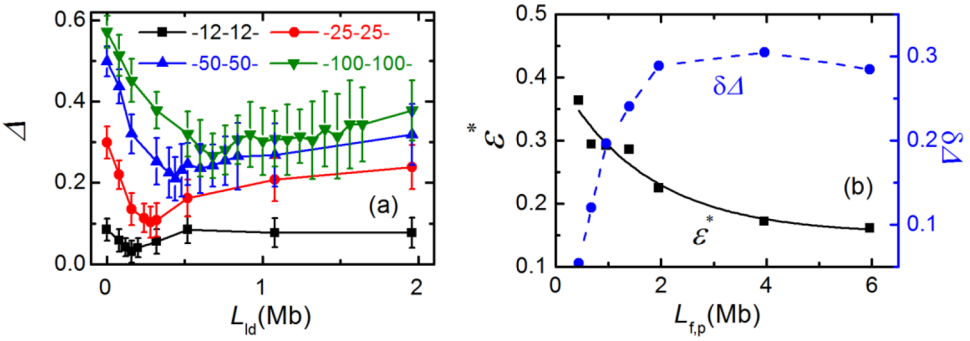

Figure 3. (a) Dependence of Δ on L_{ld} at A_{sp} = 160 for polymers of different F/P lengths $L_{f,p}$. (b) Dependence of critical length ratio $\varepsilon^* = L_{ld}^*/L_{f,p}$ and the maximum difference of phase separation $\delta\Delta = \Delta(L_{ld} = 0) - \Delta(L_{ld} = L_{ld}^*)$ on $L_{f,p}$.

with curvilinear distance $S < L_{ld}$ are neglected to remove its effect on P^{same}, which could be non-negligible for short polymers. Similar simulation conditions and post-measurements are implemented to simulate either single human chromosome 1 (Chr1) or two interacting human chromosomes (Chr1+Chr2).

RESULTS

Single $-n_f-n_p-$ Polymer. The dependence of the order parameter for phase separation of f and p compartments, Δ, on A_{sp} for a −50−50− polymer is presented in Figure 2a. For polymer of any given length of LDs, L_{ld}, the value of Δ increases with A_{sp} and saturates at around A_{sp} = 160. For polymer without LDs (L_{ld} = 0), p beads are more likely to aggregate into clusters. Formation of a pearl necklace structure and a large crumple globule of p beads are observed respectively at A_{sp} = 155 and A_{sp} = 170. For polymers with LDs, the growth rate of Δ with the increase of A_{sp} becomes slower, and the saturated degree of phase separation Δ_{sat} at A_{sp} ≥ 160 becomes smaller. After phase separation, crumple globules of nonspherical shape are observed for 1.16 Mb ≥ L_{ld} ≥ 160 kb, due to an increased chain rigidity (see the Supporting Information).

The results also indicate that Δ depends nonmonotonically on L_{ld} at fixed A_{sp}. As shown in Figure 2b, Δ first decreases and then mildly increases with L_{ld} at A_{sp} = 160. The degree of phase separation is minimized at the critical LD length L_{ld}^* = 440 kb. We note that such nonmonotonic relation is not an artifact caused by the definition of Δ, as similar results are obtained with another choice of order parameter for phase separation (see the Supporting Information). Since the only term that drives phase separation in our model is the hydrophobicity of p beads, the variation of Δ should be attributed to the competition of surface energy and elastic energy. This could be demonstrated by the minimum at L_{ld}^* for the variation of polymeric energy and solvation energy (see the Supporting Information). The peak position of gyration radius of prairie beads R_p is also presented in Figure 2b, which perfectly agrees with the critical length at L_{ld}^* = 440 kb. The inverse correlation of R_p and Δ suggests the collapsing degree of prairie beads could serve as an order parameter for phase separation of the polymer.

Figure 3a presents the dependence of Δ on L_{ld} at A_{sp} = 160 for polymers with various F/P lengths $L_{f,p}$. The significant decrease of Δ with $L_{f,p}$ for any given L_{ld} indicates polymers of shorter blocks are more difficult to phase separate. Interestingly, the critical LD length L_{ld}^*, at which Δ is minimized, positively correlates with $L_{f,p}$. The critical length ratio $\varepsilon^* = L_{ld}^*/L_{f,p}$ is not constant at short $L_{f,p}$. As presented in Figure 3b, ε^* decays exponentially with $L_{f,p}$, which can be fitted as

$$\varepsilon^* = 0.25\, e^{-L_{f,p}/L_0} + \varepsilon_0 \quad (7)$$

with L_0 = 1.70 the decaying length, and ε_0 = 0.15 the constant ratio for sufficiently large $L_{f,p}$. Such correlation underscores the significant influence of segmental rigidity (rather than global elasticity) on phase separation. The maximum difference in phase separation $\delta\Delta = \Delta(L_{ld} = 0) - \Delta(L_{ld} = L_{ld}^*)$ also increases with $L_{f,p}$ and saturates at around 0.3 for $L_{f,p}$ ≥ 1.96 Mb, as shown in Figure 3b. The interaction parameters (namely, the bond stiffness K and repulsive parameters A) exert very limited impact on L_{ld}^*. See the Supporting Information for more details.

Two −50−50− Polymers. Figure 4a presents the order parameter for territorialization of two −50−50− polymers, Ω,

https://doi.org/10.1021/acs.jpcb.1c03523
J. Phys. Chem. B XXXX, XXX, XXX−XXX

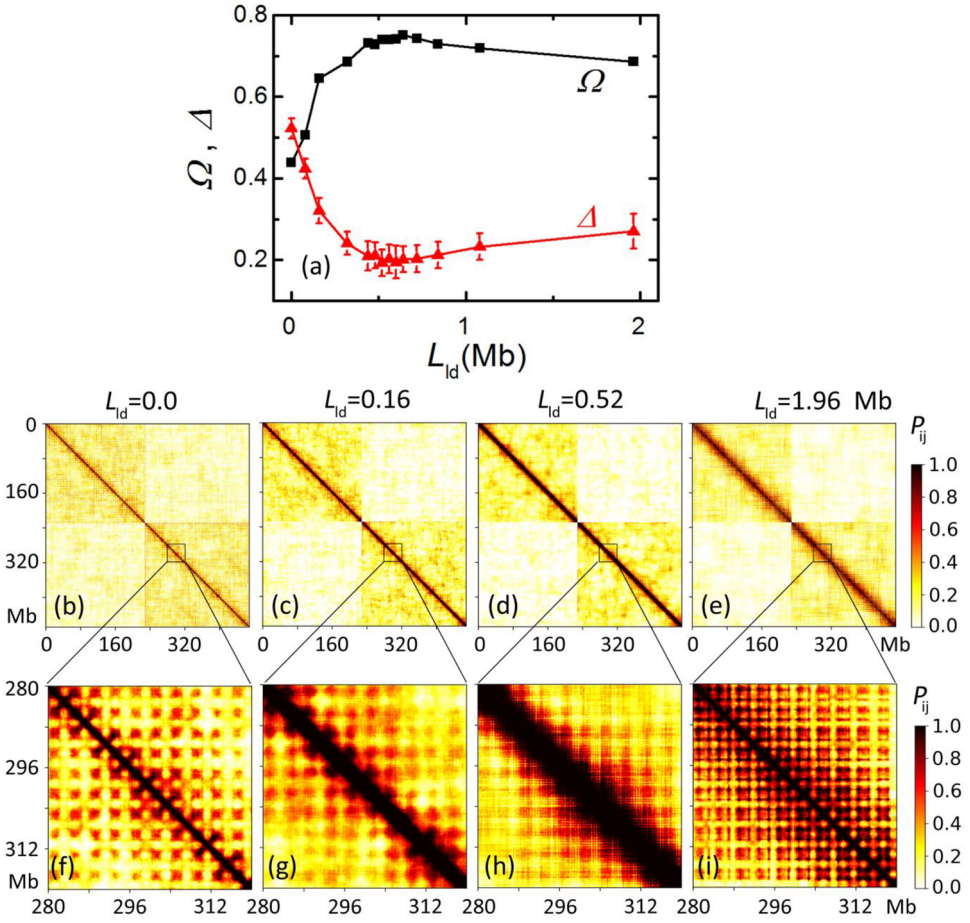

Figure 4. (a) Degree of territorialization Ω and the degree of phase separation Δ for two −50−50− polymers as a function of L_{ld} at A_{sp} = 170. (b−i) Contact maps for two −50−50− polymers with (b, f) L_{ld} = 0.0, (c,g) L_{ld} = 0.16, (d, h) L_{ld} = 0.52, and (e, i) L_{ld} = 1.96 (in unit of Mb) at A_{sp} = 170. A cutoff r_c^{map} = 6.0 is chosen for the measurement of contact pairs.

as a function of L_{ld} at A_{sp} = 170. It is observed that Ω grows rapidly when L_{ld} is increased from 0 to 520 kb. However, for L_{ld} > 640 kb, Ω slightly decreases with L_{ld}. The result indicates that loop domains at critical length (L_{ld}^{*} ∼ 520 kb) help promote the formation of territories between two polymers. This can also be demonstrated by the contact map shown in Figure 4b−e: Although distinguishable boundaries of the territory can be observed for any chosen L_{ld}, the highest contrast of intrapolymeric to interpolymeric contact probability is obtained for polymers with L_{ld} = 520 kb.

Figure 4a also presents the degree of phase separation Δ of the two-polymer system. It can be seen that Δ first decreases and then slightly increases with L_{ld}. The same turning point is obtained at around L_{ld}^{*} = 520 kb for both Δ and Ω. This indicates that the nonmonotonic Ω−L_{ld} relation could be attributed to the change in the degree of phase separation. In fact, the degree of interpolymeric aggregation is negatively correlated to the degree of intrapolymeric phase separation: For L_{ld} < L_{ld}^{*}, while the probability of interpolymeric contact, P^{diff}, decreases with L_{ld}, the probability of intrapolymeric contact, P^{same}, is significantly increased. Such correlations are reversed for L_{ld} > L_{ld}^{*} (see the Supporting Information). Figure 4f−i also presents a zoom in view of the diagonal region for segment from 280 to 320 Mb. The checkerboard-like patterns with clear boundaries formed by periodic f and p blocks can be easily discerned for L_{ld} = 0.0 and 1.96 Mb. By contrast, those boundaries become significantly blurred for L_{ld} = 520 kb and thus become fuzzier at further distance from the main diagonal. The critical length for the two-polymer system L_{ld}^{*} = 520 kb is slightly larger than that for a single −50−50− polymer (i.e., L_{ld}^{*} = 440 kb). This could be attributed to the depletion effect: the decrease in solvation energy from phase separation is significantly larger for the two-polymer system than that for a single polymer, especially for L_{ld} > L_{ld}^{*} (see the Supporting Information).

Human Chromosomes. The TAD lengths L_{tad} and F/P lengths $L_{f,p}$ for human chromosome 1 (Chr1) and 2 (Chr2) are of Gamma distributions (Γ), as presented in Figure 5a−d (similar distributions are also obtained for other human chromosomes; see the Supporting Information). As indicated by the dashed lines in Figure 5a,c, the mean lengths of F/P $\overline{L_{f,p}}$ = 1.60 Mb for Chr1 and $\overline{L_{f,p}}$ = 2.02 Mb for Chr2. Interestingly, the corresponding mean lengths of TADs shown in Figure 5b,d for chromosomes taken from H1 cell lines[50] ($\overline{L_{tad}}$ = 0.46 Mb for Chr1 and $\overline{L_{tad}}$ = 0.51 Mb for Chr2) are very close to the critical LD length L_{ld}^{*} predicted by eq 7 by substituting $L_{f,p}$ with $\overline{L_{f,p}}$ (i.e., L_{ld}^{*} = 0.43 Mb for Chr1 and L_{ld}^{*} = 0.49 Mb for Chr2). We also compare $\overline{L_{f,p}}$ for human Chr1−Chr22 in Figure 5e, the value of which fluctuate around 1.96 Mb. The mean lengths of TADs, $\overline{L_{tad}}$, vary across different cell lines or primary tissues,[50,51] as shown in Figure 5f. $\overline{L_{tad}}$ ∼ 0.56 Mb and $\overline{L_{tad}}$ ∼ 0.44 Mb are obtained respectively for

https://doi.org/10.1021/acs.jpcb.1c03523
J. Phys. Chem. B XXXX, XXX, XXX−XXX

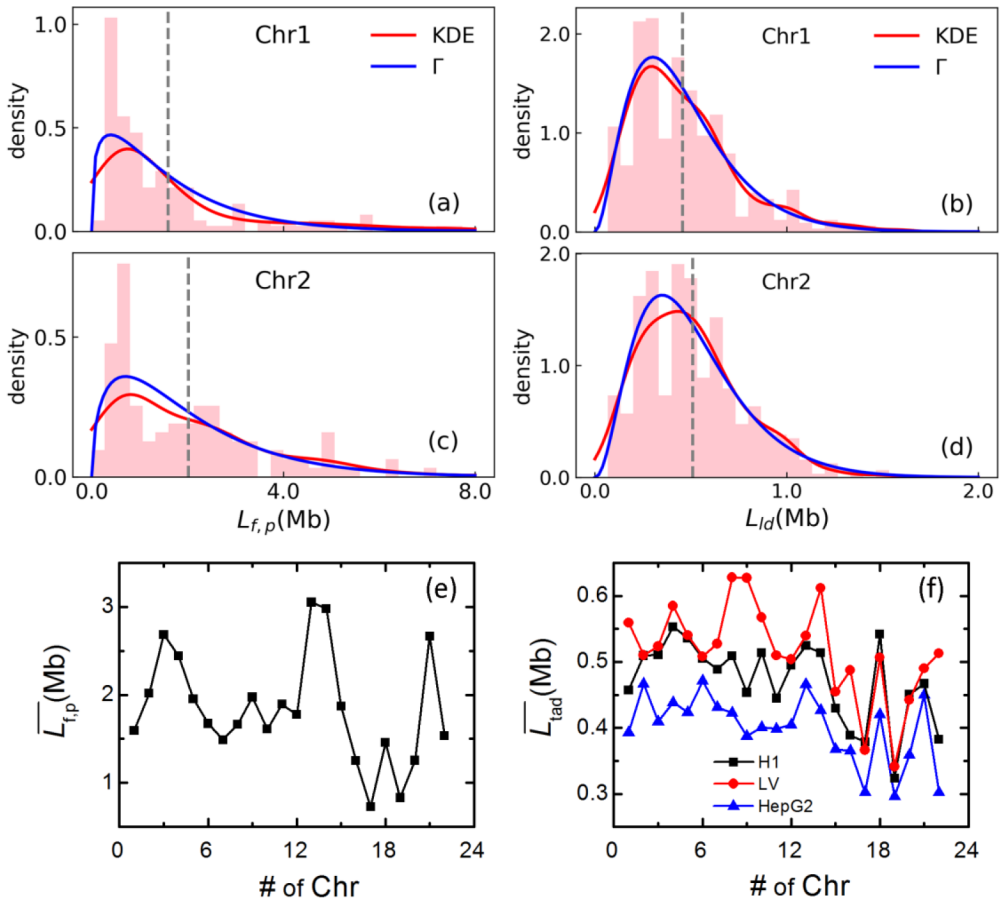

Figure 5. (a–d) Distributions of F/P lengths $L_{f,p}$ and TAD lengths L_{tad} from H1[50] for Chr1 and Chr2. The dashed line indicates the mean lengths: $\overline{L_{f,p}} = 1.60$ and $\overline{L_{tad}} = 0.46$ for Chr1; $\overline{L_{f,p}} = 2.02$ and $\overline{L_{tad}} = 0.51$ for Chr2 (in Mb). Solid lines are fitting curves of kernel density estimation (KDE) and Gamma distributions (Γ). (e) Mean lengths $\overline{L_{f,p}}$ for Chr1–Chr22. (f) Mean lengths $\overline{L_{tad}}$ for Chr1–Chr22 taken from different cell lines or tissues.[50,51]

chromosomes taken from LV (liver cells) and HepG2 (liver cancer cells), which implies shortened TADs in oncogenesis. The variance of L_{tad} is larger for chromosomes taken from LV than that taken from HepG2 (Figure S2), which possibly makes the former less sensitive to stimuli.[58]

Figure 6 provides the ratio of the mean TAD and F/P lengths $\varepsilon = \overline{L_{tad}}/\overline{L_{f,p}}$ for Chr1–Chr22. Similar trends of the variation of ε across different chromosomes (e.g., a dip at Chr3 and a sharp peak at Chr17) demonstrate its conservation in different cell lines or tissues. In fact, the three groups of $\overline{L_{tad}}$ have a moderately linear correlation with $\overline{L_{f,p}}$, with Pearson's correlation coefficient fluctuating around 0.6 (see the Supporting Information).

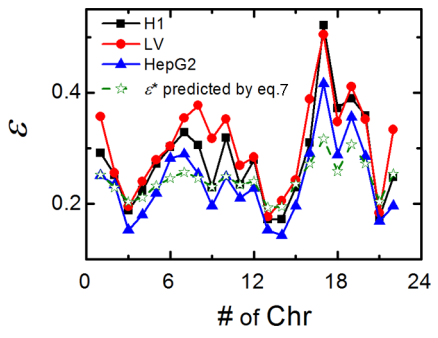

Figure 6. Ratio of the mean TAD and F/P lengths $\varepsilon = \overline{L_{tad}}/\overline{L_{f,p}}$ and the critical length ratio to minimize phase separation $\varepsilon^* = L_{ld}^*/\overline{L_{f,p}}$ derived from eq 7 (green stars), for Chr1–Chr22.

Interestingly, the critical length ratio to minimize phase separation $\varepsilon^* = L_{ld}^*/\overline{L_{f,p}}$ determined by eq 7 follows the same trend, the magnitude of which is very close to ε for various chromosomes, as indicated by green stars in Figure 6. The results also indicate the following: (1) $\overline{L_{tad}}$ is positively correlated to $\overline{L_{f,p}}$ with ratio ε fluctuating around 0.3 for all human chromosomes. (2) ε decays exponentially with $\overline{L_{f,p}}$, which can be approximated with eq 7 by substituting $L_{f,p}$ with $\overline{L_{f,p}}$. (3) TADs (or ε) for this type of malignant liver cells (HepG2) are evidently smaller than that for noncancerous liver cells (LV).

TADs are of a hierarchic structure with small loops forming inside bigger ones.[59] These loops are dynamic, being generated and opened repeatedly in real time. We expect limited influence of these dynamics on the equilibrium configurations of the entire chain (and thus the degree of phase separation) and treat TAD boundaries as self-constrained LDs in our simulations. Chromosome is thus expected to be more phase-separated at larger difference $\delta\varepsilon = |\varepsilon - \varepsilon^*|$ (e.g., Chr1 for LV and Chr3 for HepG2). To check this, in Figure 7a we present

https://doi.org/10.1021/acs.jpcb.1c03523
J. Phys. Chem. B XXXX, XXX, XXX−XXX

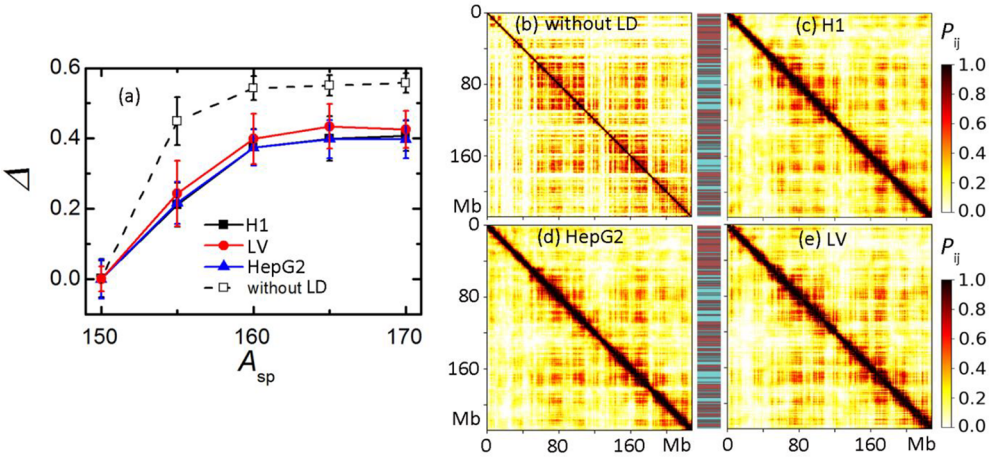

Figure 7. (a) Degree of phase separation Δ as a function of A_{sp}, for Chr1. (b−e) Contact map for Chr1 (b) without LD, and with LD boundaries derived from (c) H1, (d) HepG2, or (e) LV, at A_{sp} = 160. The cutoff radius for mapping r_c^{map} was 6.0.

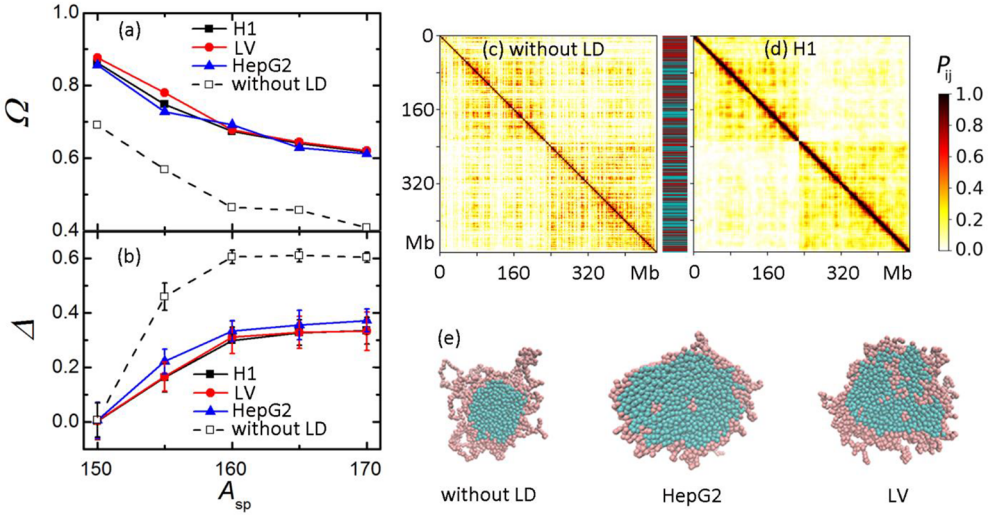

Figure 8. (a) Degree of territorialization Ω and (b) degree of phase separation Δ as a function of A_{sp} for Chr1+Chr2 with different LD boundaries. (c, d) Contact map for Chr1+Chr2 (c) without LD or (d) with LD boundaries from H1 at A_{sp} = 160 (utoff radius for mapping r_c^{map} = 6.0). (e) Sectional views of simulation snapshots for Chr1+Chr2 with different LD boundaries.

simulation results of the order parameter Δ as a function of A_{sp} for polymer with distributions of $L_{f,p}$ and L_{ld} determined respectively by genomic sequence and Hi-C data of Chr1. Similar to the results for the −50−50− polymer, the saturated degree of compartmentalization Δ_{sat} is obtained at $A_{sp} \geq 160$, and Δ_{sat} is larger for system without LD (i.e., $L_{ld} = 0$). We find Δ_{sat} for Chr1 from LV to be slightly larger than that for Chr1 from HepG2 or H1, which follows the prediction of Figure 6.

The checkerboard-like pattern of phase separation can be visualized by the contact map shown in Figure 7b−e. The decrease of Δ is manifested by the blurring of the boundaries for phase separation of Chr1. By comparing Figure 7d,e, we also find Chr1 from HepG2 with shortened TADs are of higher intra-TAD but lower inter-TAD contact probabilities (i.e., darker but less blurred diagonal).

The dependence of order parameter for interchromosomal territorialization Ω and phase separation Δ for two interacting human chromosomes (Chr1+Chr2) on A_{sp} is shown in Figure 8a,b. Similar to the one-polymer system, we find that Δ increases with A_{sp} and saturates at around A_{sp} = 160. By contrast, Ω decreases monotonically with A_{sp}, with smaller rate of descent for A_{sp} > 160. We note that the probability of both intrachromosomal contact P^{same} and interchromosomal contact P^{diff} increase with A_{sp}, but a faster growth rate is observed for P^{diff} (see the Supporting Information), resulting in lower degree of territorialization at higher A_{sp}. The contact maps for Chr1+Chr2 are presented in Figure 8c,d. While very clear boundaries of chromosomal territories are observed for system with LDs, for polymers without LD the boundaries can hardly be distinguished due to strong phase separation. For $A_{sp} \geq 160$, Ω are almost indistinguishable for Chr1+Chr2 with LD boundaries taken from different cell lines or tissues, but a slightly larger Δ is obtained for polymers with LD boundaries taken from HepG2, as shown in Figure 8b. This result is different from the one-polymer system shown in Figure 7a, where Δ is larger for Chr1 taken from LV than that taken from HepG2. As mentioned in our analysis on polymers of periodic blocks, the critical length ratio ε^* becomes larger for the two-polymer system compared to that for a single polymer due to depletion effect. We thus obtain smaller degree of phase separation for Chr1+Chr2 taken from LV and H1 (with smaller difference $\delta\varepsilon = |\varepsilon - \varepsilon^*|$), which is consistent with Δ

https://doi.org/10.1021/acs.jpcb.1c03523
J. Phys. Chem. B XXXX, XXX, XXX−XXX

determined experimentally from Hi-C data (Table 2). This argument is also supported by the sectional view of simulation snapshots in Figure 8e: The number of f beads buried inside the large crumple globule of p beads is greater for Chr1+Chr2 taken from LV than that taken from HepG2. The number of buried f beads is still much larger than that for system without LDs so that shortened LDs only slightly elevate the degree of phase separation for Chr1+Chr2.

Table 2. Comparison of Δ Determined from Hi-C Data and Simulations[a]

data sources	no. of Chr	LV	HepG2	H1
Hi-C[b]	Chr1	0.21	0.29	0.24
	Chr2	0.20	0.23	0.20
simulations	Chr1+Chr2	0.33	0.37	0.34

[a]See the Supporting Information for how to measure Δ from Hi-C data. [b]Hi-C data for LV and H1 are derived from ref 50 and data for HepG2 are derived from ref 51.

CONCLUDING REMARKS

The multiscale structures enable chromosomes to fold inside the cell nucleus with high compaction and easy unentanglement. We in this work implement a coarse-grained model of chromosomes as block copolymers to investigate the interplay of different folding strategies, namely, topological constraints, intrachromosomal compartments, and interchromosomal territories, with a focus on the effect of the length of loop domains (LDs) on phase separation and territory formation. For polymer of periodic blocks, a critical LD length L_{ld}^{*} that minimizes the degree of phase separation is determined. This originates from the nonmonotonic dependence of segmental rigidity on LD length. Due to the depletion effect, a slightly larger L_{ld}^{*} that can not only maximize the degree of territorialization but also minimize the degree of phase separation is determined for the two-polymer system. The peak positions for the gyration radius of prairie beads also agree well with L_{ld}^{*} for both systems. The results indicate that topological constraints with optimal length can promote the formation of territories by weakening the degree of phase separation.

L_{ld}^{*} is positively correlated to the length of F/P segments $L_{f,p}$ of the polymer, and the ratio $\epsilon^{*} = L_{ld}^{*}/L_{f,p}$ decays exponentially with $L_{f,p}$ (eq 7). Interestingly, we find this correlation applies to human chromosomes by comparing with experimental data: The mean lengths of TADs for all human chromosomes are close to the critical value L_{ld}^{*} and positively correlate with the mean length of F/P segments, which is consistent with the prediction of eq 7. The biological implications of this correlation may lie in better formation of territories and easier unfolding during transcription. As relocation of the genome may influence their functioning, it might be important to promote the formation of territories. This allows the change of spatial organization of chromosomes in response to regulation.[23,24] The formation of territories also attenuates the translocation potential of cells[25] and prevents abnormal clustering of heterochromatin domains.[26] Meanwhile, there will be less energy cost required to unfold chromosomal fiber into more flexible configurations during transcription, especially for inactive genes (e.g., stress-response genes). This coincides with the spatial intermingling of F/P segments, which is cell-type specific and increases during differentiation.[16,17]

The biological significance of the wide distribution of TAD lengths could be manifold. On the basis of previous studies[58] and our simulations, such a wide distribution prevents sharp changes in structure in response to stimuli, while it maintains the formation of territories. Moreover, giant loops can protrude far from the chromosome territory and intermingle extensively with fibers from neighboring chromosomes for genetic "cross-talk".[3,24,60] The wide distribution of F/P lengths makes the chromosome a blocky-random copolymer[61−64] of chemical, physical, and mechanical heterogeneity. The more randomly distributed segments tend to wrap around prairie-rich blocky segments, providing stability against coagulation with neighboring chromosomes even in the absence of TADs.

ASSOCIATED CONTENT

Supporting Information

The Supporting Information is available free of charge at https://pubs.acs.org/doi/10.1021/acs.jpcb.1c03523.

Modeling for human chromosomes, conversion of units, analysis on polymers at swollen state, measuring compartmentalization based on graph theory, effect of interaction parameters, shape of collapsed polymers, potential energy for $-n_f-n_p-$ polymers, determination of Δ from Hi-C data, further discussions on P^{same} and P^{diff}, and effect of heterogeneous loop sizes (PDF)

AUTHOR INFORMATION

Corresponding Authors

Jiachen Wei − *State Key Laboratory of Nonlinear Mechanics and Beijing Key Laboratory of Engineered Construction and Mechanobiology, Institute of Mechanics, Chinese Academy of Sciences, Beijing 100190, China; Shenzhen Bay Laboratory, 518055 Shenzhen, Guangdong, China;* orcid.org/0000-0003-3802-5310; Email: weijiachen@lnm.imech.ac.cn

Yi Qin Gao − *Shenzhen Bay Laboratory, 518055 Shenzhen, Guangdong, China; Beijing National Laboratory for Molecular Sciences, College of Chemistry and Molecular Engineering, Biomedical Pioneering Innovation Center (BIOPIC), and Beijing Advanced Innovation Center for Genomics (ICG), Peking University, Beijing 100871, China;* orcid.org/0000-0002-4309-9376; Email: gaoyq@pku.edu.cn

Authors

Hao Tian − *Beijing National Laboratory for Molecular Sciences, College of Chemistry and Molecular Engineering, Biomedical Pioneering Innovation Center (BIOPIC), and Beijing Advanced Innovation Center for Genomics (ICG), Peking University, Beijing 100871, China*

Rui Zhou − *Beijing National Laboratory for Molecular Sciences, College of Chemistry and Molecular Engineering, Biomedical Pioneering Innovation Center (BIOPIC), and Beijing Advanced Innovation Center for Genomics (ICG), Peking University, Beijing 100871, China*

Yingfeng Shao − *State Key Laboratory of Nonlinear Mechanics and Beijing Key Laboratory of Engineered Construction and Mechanobiology, Institute of Mechanics, Chinese Academy of Sciences, Beijing 100190, China; School of Engineering Science, University of Chinese Academy of Sciences, Beijing 100049, China*

https://doi.org/10.1021/acs.jpcb.1c03523
J. Phys. Chem. B XXXX, XXX, XXX−XXX

Fan Song − *State Key Laboratory of Nonlinear Mechanics and Beijing Key Laboratory of Engineered Construction and Mechanobiology, Institute of Mechanics, Chinese Academy of Sciences, Beijing 100190, China; School of Engineering Science, University of Chinese Academy of Sciences, Beijing 100049, China;* orcid.org/0000-0001-7359-2519

Complete contact information is available at: https://pubs.acs.org/10.1021/acs.jpcb.1c03523

Notes

The authors declare no competing financial interest.

■ ACKNOWLEDGMENTS

This work was supported by NSFC Basic Science Center Program for "Multiscale Problems in Nonlinear Mechanics" (grant no.11988102 to F.S.), National Natural Science Foundation of China (grant nos. 92053202 and 22050003 to Y.Q.G.) and the Strategic Priority Research Program of the Chinese Academy of Sciences (grant no. XDB22040102 to F.S.).

■ REFERENCES

(1) Parmar, J. J.; Woringer, M.; Zimmer, C. How the genome folds: the biophysics of four-dimensional chromatin organization. *Annu. Rev. Biophys.* **2019**, *48*, 231−253.
(2) Moller, J.; de Pablo, J. J. Bottom-up meets top-down: the crossroads of multiscale chromatin modeling. *Biophys. J.* **2020**, *118*, 2057−2065.
(3) Mirny, L. A. The fractal globule as a model of chromatin architecture in the cell. *Chromosome Res.* **2011**, *19*, 37−51.
(4) Mirny, L. A.; Imakaev, M.; Abdennur, N. Two major mechanisms of chromosome organization. *Curr. Opin. Cell Biol.* **2019**, *58*, 142−152.
(5) Zheng, H.; Xie, W. The role of 3d genome organization in development and cell differentiation. *Nat. Rev. Mol. Cell Biol.* **2019**, *20*, 535−550.
(6) Halverson, J. D.; Smrek, J.; Kremer, K.; Grosberg, A. Y. From a melt of rings to chromosome territories: the role of topological constraints in genome folding. *Rep. Prog. Phys.* **2014**, *77*, 022601.
(7) Wang, S.; Su, J. H.; Beliveau, B. J.; Bintu, B.; Moffitt, J. R.; Wu, C. T.; Zhuang, X. Spatial organization of chromatin domains and compartments in single chromosomes. *Science* **2016**, *353*, 598−602.
(8) Szabo, Q.; Bantignies, F.; Cavalli, G. Principles of genome folding into topologically associating domains. *Sci. Adv.* **2019**, *5*, eaaw1668.
(9) Bendandi, A.; Dante, S.; Zia, S. R.; Diaspro, A.; Rocchia, W. Chromatin compaction multi-scale modeling: A complex synergy between theory, simulation, and experiment. *Front. Mol. Biosci.* **2020**, *7*, 00015.
(10) Erdel, F. Biophysical mechanisms of chromatin patterning. *Curr. Opin. Genet. Dev.* **2020**, *61*, 62−68.
(11) Conte, M.; Fiorillo, L.; Bianco, S.; Chiariello, A. M.; Esposito, A.; Nicodemi, M. Polymer physics indicates chromatin folding variability across single-cells results from state degeneracy in phase separation. *Nat. Commun.* **2020**, *11*, 3289.
(12) Fudenberg, G.; Imakaev, M.; Lu, C.; Goloborodko, A.; Abdennur, N.; Mirny, L. A. Formation of chromosomal domains by loop extrusion. *Cell Rep.* **2016**, *15*, 2038−49.
(13) Lieberman-Aiden, E.; Van Berkum, N. L.; Williams, L.; Imakaev, M.; Ragoczy, T.; Telling; Amit, A. I.; Lajoie, B. R.; Sabo, P. J.; Dorschner, M. O.; et al. Comprehensive mapping of long-range interactions reveals folding principles of the human genome. *Science* **2009**, *326*, 289−93.
(14) Nuebler, J.; Fudenberg, G.; Imakaev, M.; Abdennur, N.; Mirny, L. A. Chromatin organization by an interplay of loop extrusion and compartmental segregation. *Proc. Natl. Acad. Sci. U. S. A.* **2018**, *115*, E6697−E6706.
(15) Falk, M.; Feodorova, Y.; Naumova, N.; Imakaev, M.; Lajoie, B. R.; Leonhardt, H.; Joffe, B.; Dekker, J.; Fudenberg, G.; Solovei, I.; Mirny, L. A. Heterochromatin drives compartmental-ization of inverted and conventional nuclei. *Nature* **2019**, *570*, 395−399.
(16) Liu, S.; Zhang, L.; Quan, H.; Tian, H.; Meng, L.; Yang, L.; Feng, H.; Gao, Y. Q. From 1d sequence to 3d chromatin dynamics and cellular functions: A phase separation perspective. *Nucleic Acids Res.* **2018**, *46*, 9367−9383.
(17) Quan, H.; Yang, Y.; Liu, S.; Tian, H.; Xue, Y.; Gao, Y. Q. Chromatin structure changes during various processes from a DNA sequence view. *Curr. Opin. Struct. Biol.* **2020**, *62*, 1−8.
(18) Brackey, C. A.; Marenduzzo, D.; Gilbert, N. Mechanistic modeling of chromatin folding to understand function. *Nat. Methods* **2020**, *17*, 767−775.
(19) MacPherson, Q.; Beltran, B.; Spakowitz, A. J. Bottom−up modeling of chromatin segregation due to epigenetic modifications. *Proc. Natl. Acad. Sci. U. S. A.* **2018**, *115*, 12739−12744.
(20) Strom, A. R.; Emelyanov, A. V.; Mir, M.; Fyodorov, D. V.; Darzacq, X.; Karpen, G. H. Phase separation drives heterochromatin domain formation. *Nature* **2017**, *547*, 241−245.
(21) Guthmann, M.; Burton, A.; Torres-Padilla, M. E. Expression and phase separation potential of heterochromatin proteins during early mouse development. *EMBO Rep.* **2019**, *20*, e47952.
(22) Cremer, T.; Cremer, M. Chromosome territories. *Cold Spring Harbor Perspect. Biol.* **2010**, *2*, a003889.
(23) Cremer, T.; Cremer, M.; Dietzel, S.; Müller, S.; Solovei, I.; Fakan, S. Chromosome territories−a functional nuclear landscape. *Curr. Opin. Cell Biol.* **2006**, *18*, 307−316.
(24) Meaburn, K. J.; Misteli, T. Chromosome territories. *Nature* **2007**, *445*, 379−381.
(25) Rosin, L. F.; Crocker, O.; Isenhart, R. L.; Nguyen, S. C.; Xu, Z.; Joyce, E. F. Chromosome territory formation attenuates the translocation potential of cells. *eLife* **2019**, *8*, e49553.
(26) Hoencamp, C.; Dudchenko, O.; Elbatsh, A. M.; Brahmachari, S.; Raaijmakers, J. A.; van Schaik, T.; Sedeño Cacciatore, A. S.; Contessoto, V. G.; van Heesbeen, R.; van den Broek, B.; et al. 3D genomics across the tree of life reveals condensin II as a determinant of architecture type. *Science* **2021**, *372*, 984−989.
(27) Ganai, N.; Sengupta, S.; Menon, G. I. Chromosome positioning from activity-based segregation. *Nucleic Acids Res.* **2014**, *42*, 4145−4159.
(28) Di Pierro, M.; Potoyan, D. A.; Wolynes, P. G.; Onuchic, J. N. Anomalous diffusion, spatial coherence, and viscoelasticity from the energy landscape of human chromosomes. *Proc. Natl. Acad. Sci. U. S. A.* **2018**, *115*, 7753−7758.
(29) Shaban, H. A.; Barth, R.; Recoules, L.; Bystricky, K. Hi-D: Nanoscale mapping of nuclear dynamics in single living cells. *Genome Biol.* **2020**, *21*, 95.
(30) Shi, G.; Liu, L.; Hyeon, C.; Thirumalai, D. Interphase human chromosome exhibits out of equilibrium glassy dynamics. *Nat. Commun.* **2018**, *9*, 3161.
(31) Tamm, M. V.; Nazarov, L. I.; Gavrilov, A. A.; Chertovich, A. V. Anomalous diffusion in fractal globules. *Phys. Rev. Lett.* **2015**, *114*, 178102.
(32) Rao, S. S.; Huang, S.-C.; Glenn St Hilaire, B. G.; Engreitz, J. M.; Perez, E. M.; Kieffer-Kwon, K. R.; Sanborn, A. L.; Johnstone, S. E.; Bascom, G. D.; Bochkov, I. D.; et al. Cohesin loss eliminates all loop domains. *Cell* **2017**, *171*, 305−320.
(33) Schwarzer, W.; Abdennur, N.; Goloborodko, A.; Pekowska, A.; Fudenberg, G.; Loe-Mie, Y.; Fonseca, N. A.; Huber, W.; Haering, C. H.; Mirny, L.; et al. Two independent modes of chromatin organization revealed by cohesin removal. *Nature* **2017**, *551*, 51−56.
(34) Haarhuis, J. H.; van der Weide, R. H.; Blomen, V. A.; Yáñez-Cuna, J. O.; Amendola, M.; van Ruiten, M. S.; Krijger, P. H.; Teunissen, H.; Medema, R. H.; van Steensel, B.; et al. The cohesin release factor WAPL restricts chromatin loop extension. *Cell* **2017**, *169*, 693−707.

(35) Imakaev, M. V.; Tchourine, K. M.; Nechaev, S. K.; Mirny, L. A. Effects of topological constraints on globular polymers. *Soft Matter* **2015**, *11*, 665−71.
(36) Smrek, J.; Grosberg, A. Y. Understanding the dynamics of rings in the melt in terms of the annealed tree model. *J. Phys.: Condens. Matter* **2015**, *27*, 064117.
(37) Qi, Y.; Reyes, A.; Johnstone, S. E.; Aryee, M. J.; Bernstein, B. E.; Zhang, B. Data-driven polymer model for mechanistic exploration of diploid genome organization. *Biophys. J.* **2020**, *119*, 1905−1916.
(38) Zhang, B.; Wolynes, P. G. Topology, structures, and energy landscapes of human chromosomes. *Proc. Natl. Acad. Sci. U. S. A.* **2015**, *112*, 6062−6067.
(39) Zhou, R.; Gao, Y. Q. Polymer models for the mechanisms of chromatin 3D folding: review and perspective. *Phys. Chem. Chem. Phys.* **2020**, *22*, 20189−20201.
(40) Fiorillo, L.; Bianco, S.; Esposito, A.; Conte, M.; Sciarretta, R.; Musella, F.; Chiariello, A. M. A modern challenge of polymer physics: Novel ways to study, interpret, and reconstruct chromatin structure. *Wiley Interdiscip. Rev.: Comput. Mol. Sci.* **2020**, *10*, e1454.
(41) Haddad, N.; Jost, D.; Vaillant, C. Perspectives: Using polymer modeling to understand the formation and function of nuclear compartments. *Chromosome Res.* **2017**, *25*, 35−50.
(42) Bianco, S.; Chiariello, A. M.; Conte, M.; Esposito, A.; Fiorillo, L.; Musella, F.; Nicodemi, M. Computational approaches from polymer physics to investigate chromatin folding. *Curr. Opin. Cell Biol.* **2020**, *64*, 10−17.
(43) Jost, D.; Carrivain, P.; Cavalli, G.; Vaillant, C. Modeling epigenome folding: Formation and dynamics of topologically associated chromatin domains. *Nucleic Acids Res.* **2014**, *42*, 9553−61.
(44) Brackley, C. A.; Johnson, J.; Kelly, S.; Cook, P. R.; Marenduzzo, D. Simulated binding of transcription factors to active and inactive regions folds human chromosomes into loops, rosettes and topological domains. *Nucleic Acids Res.* **2016**, *44*, 3503−12.
(45) Chertovich, A.; Kos, P. Crumpled globule formation during collapse of a long flexible and semiflexible polymer in poor solvent. *J. Chem. Phys.* **2014**, *141*, 134903.
(46) Gavrilov, A. A.; Shevelyov, Y. Y.; Ulianov, S. V.; Khrameeva, E. E.; Kos, P.; Chertovich, A.; Razin, S. V. Unraveling the mechanisms of chromatin fibril packaging. *Nucleus* **2016**, *7*, 319−24.
(47) Petrov, A.; Kos, P.; Chertovich, A. Kinetic mechanisms of crumpled globule formation. *Soft Matter* **2020**, *16*, 2045−2054.
(48) Ulianov, S. V.; Doronin, S. A.; Khrameeva, E. E.; Kos, P. I.; Luzhin, A. V.; Starikov, S. S.; Galitsyna, A. A.; Nenasheva, V. V.; Ilyin, A. A.; Flyamer, I. M.; et al. Nuclear lamina integrity is required for proper spatial organization of chromatin in drosophila. *Nat. Commun.* **2019**, *10*, 1176.
(49) Zhou, R.; Gao, Y. Q. A DNA sequence based polymer model for chromatin folding. *Int. J. Mol. Sci.* **2021**, *22*, 1328.
(50) Schmitt, A. D.; Hu, M.; Jung, I.; Xu, Z.; Qiu, Y.; Tan, C. L.; Li, Y.; Lin, S.; Lin, Y.; Barr, C. L.; et al. A compendium of chromatin contact maps reveals spatially active regions in the human genome. *Cell Rep.* **2016**, *17*, 2042−2059.
(51) Yardımcı, G. G.; Ozadam, H.; Sauria, M. E.; Ursu, O.; Yan, K. K.; Yang, T.; Chakraborty, A.; Kaul, A.; Lajoie, B. R.; Song, F.; et al. Measuring the reproducibility and quality of Hi-C data. *Genome Biol.* **2019**, *20*, 57.
(52) Groot, R. D.; Warren, P. B. Dissipative particle dynamics: Bridging the gap between atomistic and mesoscopic simulation. *J. Chem. Phys.* **1997**, *107*, 4423−4435.
(53) Espanol, P.; Warren, P. B. Perspective: Dissipative particle dynamics. *J. Chem. Phys.* **2017**, *146*, 150901.
(54) Nikunen, P.; Vattulainen, I.; Karttunen, M. Reptational dynamics in dissipative particle dynamics simulations of polymer melts. *Phys. Rev. E Stat. Nonlin. Soft Matter Phys.* **2007**, *75*, 036713.
(55) Plimpton, S. Fast parallel algorithms for short-range molecular dynamics. *J. Comput. Phys.* **1995**, *117*, 1−19.
(56) Morlot, J.-B.; Mozziconacci, J.; Lesne, A. Network concepts for analyzing 3d genome structure from chromosomal contact maps. *EPJ. Nonlin. Biomed. Phys.* **2016**, *4*, 2.
(57) Blondel, V. D.; Guillaume, J.-L.; Lambiotte, R.; Lefebvre, E. Fast unfolding of communities in large networks. *J. Stat. Mech.: Theory Exp.* **2008**, *2008*, P10008.
(58) Negri, M.; Gherardi, M.; Tiana, G.; Cosentino Lagomarsino, M. Spontaneous domain formation in disordered copolymers as a mechanism for chromosome structuring. *Soft Matter* **2018**, *14*, 6128−6136.
(59) Rao, S. S.; Huntley, M. H.; Durand, N. C.; Stamenova, E. K.; Bochkov, I. D.; Robinson, J. T.; Sanborn, A. L.; Machol, I.; Omer, A. D.; Lander, E. S.; et al. A 3D map of the human genome at kilobase resolution reveals principles of chromatin looping. *Cell* **2014**, *159*, 1665−1680.
(60) Szczepinska, T.; Rusek, A. M.; Plewczynski, D. Intermingling of chromosome territories. *Genes, Chromosomes Cancer* **2019**, *58*, 500−506.
(61) Kenney, J. Properties of block versus random copolymers. *Polym. Eng. Sci.* **1968**, *8*, 216−226.
(62) Mao, S.; MacPherson, Q.; Qin, J.; Spakowitz, A. J. Field-theoretic simulations of random copolymers with structural rigidity. *Soft Matter* **2017**, *13*, 2760−2772.
(63) Govorun, E.; Chertovich, A. Microphase separation in random multiblock copolymers. *J. Chem. Phys.* **2017**, *146*, 034903.
(64) Sanders, C. A.; George, S. R.; Deeter, G. A.; Campbell, J. D.; Reck, B.; Cunningham, M. F. Amphiphilic block-random copolymers: self-folding behavior and stabilizers in emulsion polymerization. *Macromolecules* **2019**, *52*, 4510−4519.

https://doi.org/10.1021/acs.jpcb.1c03523
J. Phys. Chem. B XXXX, XXX, XXX−XXX